Electronic Supplementary Material (ESI) for Energy & Environmental Science.
This journal is © The Royal Society of Chemistry 2024

Supporting Information

93% Single-atom Utilization in Base-Resistant Metal-Organic Framework Quantum Dot for Ampere-level CO_2 Electroreduction

Wenpeng Ni,[a],† Xiaodong He,[b],† Houjun Chen,[a] Minyang Dai,[a] Wei Zhang,[a] Yan Zhang,[a] Shuangyin Wang,[c] and Shiguo Zhang*,[a]

[a] College of Materials Science and Engineering,
Hunan University,
Changsha 410082, China
E-mail: zhangsg@hnu.edu.cn

[b] Institute of Optoelectronics and Electromagnetic Information, School of Information Science and Engineering,
Lanzhou University,
Lanzhou, 730000, China

[c] State Key Laboratory of Chem/Bio-Sensing and Chemometrics, Advanced Catalytic Engineering Research Center of the Ministry of Education, College of Chemistry and Chemical Engineering,
Hunan University,
Changsha 410082, China

Experimental Procedures

Experimental Materials.
All reagents were commercially available and used without further purification. Propionic acid (ACS reagent, >99.5%), 1(H)-4-formayl-pyrazole (AR, 98%), Pyrrole (GC, >99.7%), Potassium carbonate (K_2CO_3, ACS, >99%), 4-methoxybenzyl chloride (PMBCl, stabilized with potassium carbonate, GC, >98%), Sodium sulfate (Reagent Plus, >99%), Cobalt (II) chloride ($CoCl_2$, metals basis, 99.7%), Ammonium cerium nitrate (CAN, metals basis, >99.99%), Nicke (II) acetate (metals basis, 99.9%), Triethylamine (GC, 99.5%), Methyl p-formylbenzoate (AR, 98%), Dichloromethane (AR, 99.5%), Magnesium sulfate (metals basis, 99.99%), Potassium hydroxide (metals basis, 99.999%), Hydrochloric acid (ACS, 37%), Zirconium chloride (metals basis, 99.9%), Benzoic acid (ACS, 99.5%) are purchased from Aladdin. Methanol (Basic resi, 99.98%), Ethyl acetate (ACS, 99%), Tetrahydrofuran (THF, AR, 99.5%), N,N-dimethylformamide (DMF, RG, 99.8%), Chloroform (AR, >99%), Acetonitrile (AR, >99%), Acetone (AR, 99.5%) are obtained from Adamas. Electrolyte solutions were prepared with deionized water (DI, 18.2 MΩ) obtained from an ultra-pure purification system (Master-S15Q, Hitech Instruments Co. Ltd., Shanghai, China).

Experimental section

Synthesis of H_4-TPP. 5,10,15,20-tetra(1H-pyrazol-4-yl)-porphyrin (H_4-TPP) was synthesized by the method described in a previous report.[1] The specific synthetic pathway can be found in Fig. S1. In brief, a three-necked flask was charged with propionic acid (100 mL) and 1(H)-4-formayl-pyrazole (4.8 g). The solution was stirred until complete dissolution of the solid chemicals, followed by refluxing. Pyrrole (0.05 mol) was then added dropwise, and the mixture was refluxed for an additional 10 hours. After cooling to room temperature, the resulting purple solid was sequentially washed with methanol, ethyl acetate, and tetrahydrofuran. ^{1}H NMR (400 MHz, DMSO-d6) δ (ppm): 13.49 (s, 4H), 9.09 (s, 8H), 8.55 (s, 8H), -2.71 (s, 2H).

Synthesis of Co-TPP. 1 mmol of H_4-TPP was dissolved in 100 mL of DMF. K_2CO_3 (1.1 g) was then added to the solution, which was heated to 70 °C. After stirring for 30 minutes, 4-methoxybenzyl chloride (0.81 mL) was added and the mixture was refluxed for an additional 2 hours at 90 °C. The solution was then cooled to room temperature and poured into ice water. The resulting products were extracted three times with $CHCl_3$ (100 mL each time), and the organic phase was dried using anhydrous Na_2SO_4. The solid residues were separated by atmospheric filtration, and the solvent was removed using rotary steaming. This process yielded a purple solid, referred to as H_4TPP-PMB. Next, 0.9 g of H_4TPP-PMB and 10 mmol of $CoCl_2$ were dissolved in 100 mL of DMF. The mixture was refluxed for 12 hours at 90 °C, and then 150 mL of water was added. The solid products were collected by filtration and washed three times with water. The products were then re-dissolved in $CHCl_3$ and washed with water three times (100 mL each time). After drying with Na_2SO_4 and removing the organic solvent, Co-TPP-PMB was obtained. To remove the protective group of PMB, 0.65 g of Co-TPP-PMB was dispersed in 100 mL of CH_3CN. Then, 15 g of ammonium cerium nitrate was added to the solution. The solution was heated at 60 °C for 5 hours, and then 70 mL of water was added. The resulting precipitate was separated and washed with $CHCl_3$, acetone, and DMF to obtain Co-TPP.

Synthesis of PCN-601(Co). In a sealed 50 mL Synthware Glass bottle, 170.4 mg of nickel acetate, 84.8 mg of Co-TPP, 424 μL of triethylamine, 1.696 mL of H_2O, and 16.96 mL of DMF were combined. After all solid chemicals dissolved, the mixture was heated in an oven at 120 °C for 24 hours. The resulting precipitate was then subjected to a series of washes using DMF, H_2O, and acetone. Subsequently, the solid was immersed in acetone for an additional 12 hours. A control sample, PCN-601, was also prepared using a similar method, but with H_4-TPP as the ligand.

Synthesis of PCN-QD. A dispersion of 30 mg of PCN-601(Co) in 10 mL of water was prepared. The solution was then subjected to sonication for 48 hours at a power of 120 W and 90% power, with a 2-second interval. To maintain a temperature below 0 °C, an ice-water bath was used. Following sonication, the precipitate was removed through centrifugation at 10000 rpm, resulting in the acquisition of a monodisperse solution of PCN-QD. The PCN-QD can be separated by freeze-drying. The PCN-QDs can be easily immobilized to activated carbon substrate via ultrasonication.

Synthesis of PCN-224(Co). Initially, 6.9 g of methyl p-formylbenzoate was dissolved in 100 mL of propionic acid at a temperature of 40 °C. Subsequently, 3 g of pyrrole was added dropwise through a pressure-equalizing dropping funnel, and the resulting solution was refluxed at 145 °C for 12 hours. The resulting solid products were sequentially washed with methanol, ethyl acetate, and tetrahydrofuran. The resulting compound, TPPCOOME, was obtained after drying (^{1}H NMR: -2.77, s, 2H; 4.15, s, 12H; 8.33, d, 8H; 8.48, d, 8H; 8.86, s, 8H). In the next step, 1.32 g of TPPCOOME and 4.79 g of cobalt chloride were added to 155 mL of DMF, and the temperature was raised to 120 °C. After 12 hours, the reaction solution was poured into 150 mL of water, and the resulting precipitate was collected and washed with water three times. The solid products were then dissolved in CH_2Cl_2 and washed with water. The organic phase was dried using $MgSO_4$. After removing the organic solvent, Co-TPPCOOME was obtained. Finally, 0.75 g of Co-TPPCOOME was dissolved in a mixture of 30 mL of tetrahydrofuran and 30 mL of methanol, and a KOH aqueous solution (2.63 g KOH, 30 mL water) was added. The resulting mixture was refluxed for 12 hours, and the organic solvent was removed under reduced pressure. Gradually, 1 M HCl was added until no solid appeared. The resulting red solid, Co-TCPP, was collected, washed with water, and vacuum dried at 80 °C.

To prepare PCN-224(Co), a mixture of 30 mg of zirconium chloride, 10 mg of Co-TCPP, and 400 mg of benzoic acid was dissolved in 2 mL of DMF and kept at 120 °C for 24 hours. The resulting solid was collected, washed with DMF, and then vacuum-dried to obtain PCN-224(Co).

Electrochemical measurements

A Biologic SP-300 workstation was used to conduct electrochemical tests. For CO_2 electroreduction, the typical air-tight, three-electrode H-type cell (30 mL, Aida Technology Development Co., Ltd, Tianjin, China) was accepted, with a Nafion membrane (117, 2.0 cm x 2.0 cm, 118.0 μm) as the separator. A platinum mesh was used as a counter electrode while a leak-free Ag/AgCl (3 M KCl) as a reference electrode. The working electrode was prepared by drop-casting catalyst ink onto carbon paper. The loading of the catalyst was 0.5 mg cm^{-2}. As for the catalyst ink, 5 mg catalyst was dispersed in an ethanol solution containing 30 μL Nafion binder (5 wt%). The electrolyte is 0.1 M $KHCO_3$, and the catholyte was purged with CO_2 gas (99.999%) for at least 30 min. The CO_2 was constantly bubbled through the catholyte during electrolysis with a flow rate of 30 sccm, controlled by a mass flow controller (HORIBA METRON). The electrolyte was stirred by a 1 cm long Taflon-coated stir bar with a speed of 500 rpm. The lid was equipped with a Teflon line extending into the electrolyte and an outlet connected to a condenser tube, whose gas outlet was directly connected with the injection line of the gas chromatography (GC). Potentiostatic electrolysis was performed with the IR compensation of 85% for reduction product collection. All potentials were converted to the RHE reference scale using the following equation:

E (vs RHE) = E (vs Ag/AgCl) + 0.197 V + 0.0591 × pH

The TOF was calculated using the following equation:

$$\mathrm{TOF} = \frac{t \times J_{total} \times \mathrm{FE/nF}}{\omega \mathrm{m_{catalyst}}/\mathrm{M}_{Co}}$$

Where t is 3600 s, J_{total} is the total current density, FE is the Faradaic efficiency of CO, n is the number of electrons involved in the reaction (n=2 for CO formation), F is the Faraday constant, w is the content of electrochemical active Co atom in the catalysts, $m_{catalyst}$ is the mass of catalyst on the working electrode, and M_{Co} is the atomic mass of Co.

The utilization efficiency of Co, defined by the proportion of active Co atoms that actually participate in the electrochemical reactions, was calculated as the following equation, and the Co atom utilization refers to the overall Co atom within the catalyst:

$$Co_{utilized}\% = \frac{\Gamma \times S \times \mathrm{M_{Co}}}{\mathrm{m_{Co\ -\ ICP}}}$$

Where Γ is the surface concentration of the electrochemical active Co atom. *S* is the geometric area of the working electrode. $m_{Co\text{-}ICP}$ is the content of the Co element acquired by ICP testing.

The surface concentration was calculated by the following equation.

$$i_{p,c} = \frac{n^2F^2vA\Gamma}{4RT}$$

Where n is the number of electrons transferred (n=1 for Co^{2+}/Co^{+} couple). F is the Faraday constant (96485 C mol^{-1}). v is the scan rate (V s^{-1}). A is the electrode area (cm^2). Γ is the surface coverage of the active site (mol cm^{-2}). R is the gas constant (8.314 J mol^{-1} k^{-1}). T is the temperature (298 K).

***Electrochemical Impedance spectroscopy (EIS) and complex capacitance analysis*.** EIS was collected by a three-electrode cell. The measurements were conducted at constant potentials in the frequency range from 50 mHz to 100 KHz with an AC amplitude of 10 mV. Based on the previous report, the complex capacitance (C') was analyzed according to the following equations.[2]

$$C^{'}(\omega) = \frac{-Z^{''}(\omega)}{\omega|Z(\omega)|^2}$$

$$C^{''}(\omega) = \frac{Z^{'}(\omega)}{\omega|Z(\omega)|^2}$$

$$Z(\omega) = \frac{1}{j\omega C(\omega)'}$$

$$C(\omega) = C^{'}(\omega) - jC''(\omega)$$

Where Z(ω) is impedance and ω is the penetration depth. C′(ω) and C″(ω) is the real part and imaginary part of the capacitance C(ω).

Flow-cell testing. A custom-designed flow cell reactor made of polymethyl methacrylate plastic was utilized for flow cell measurements. The electrochemical data were collected by a workstation equipped with a current amplifier (Chenhua, Shanghai). A gas diffusion electrode (Sigracet 29 BC) was used as a substrate for working electrode construction. The catalyst was deposited on GDE via air-spraying, forming a cathode with a catalyst loading of 1.0 mg cm^{-2}. The anode is a Pt plate, and the reference electrode of Ag/AgCl was inserted into the cathode compartment. CO_2 gas flowed over the back of GDE at the rate of 50 sccm. 1 M KOH was used as the electrolyte, which was forced to continuously circulate through the cathode compartment at a rate of 5 sccm. The anion exchange membrane is the separator. The faradaic efficiency was calculated by the outlet flow rate.

Product analysis. Gas phase products were analyzed by online GC (Shimadzu, GC-2014). The GC is equipped with one TCD detector for H_2 and CO, one flame ionization detector (FID) coupled with a methanizer for CO and CH_4 detection, and one FID for C_{2+} chemicals. Ar (99.999%) was used as carrier gas. The products collected at 1000 s were sampled into the gas sampling loop of GC (1 mL). The liquid products were detected by ^{1}H NMR. The Faradaic efficiency and partial current density of H_2 and CO were calculated as below:

$$FE_{co} = \frac{2\mathrm{F}n_{CO}}{\mathrm{Q}}$$

$$FE_{H2} = \frac{2\mathrm{F}n_{H2}}{\mathrm{Q}}$$

$j_{co} = FE_{co} \times j_{total}$

$j_{H2} = FE_{H2} \times j_{total}$

Where F is the Faraday constant (96485 C mol^{-1}). Q is the total passed charge.

Characterizations

The phase detections of the samples were performed on a D/max 2550 VB X-ray diffractometer using Cu Kα radiation (λ=0.154 nm) and the scan speed was 5 ° min^{-1}. X-ray photoelectron spectra (XPS) were measured using an ECSALAB250Xi spectrometer with an Al Kα X-ray (1486.6 eV) radiation for excitation, and the binding energy was corrected by C 1s value of 284.6 eV. Transmission electron microscopy (TEM) with a spherical aberration corrector (HRTEM, Titan G2 60-300) equipped with energy dispersive X-ray spectroscopy (EDS) mapping was used for morphology measurements, and the atomic dispersion of Fe atoms was detected by Aberration-corrected HAADF-STEM (JEM-ARM200F). N_2 adsorption-desorption measurements were conducted by volumetric adsorption analyzer (JW-BK200C, Beijing JWGB Sci.& Tech. Co., Ltd.) at 76.2 K. According to the nonlocal density functional theory (NLDFT), the pore size distributions of the samples were analyzed based on the adsorption branch of the isotherms. Raman spectra were collected by using a DXRI Raman Microscope (Thermo Fisher) with a 532-nm laser. The content of Co was characterized by inductively coupled plasma atomic emission spectroscopy (ICP-AES, ICAP 7000 SERIES). UV-vis absorption spectra were recorded on a Shimadzu UV-2600 spectrophotometer in the wavelength range of 300-800 nm. Co-K-edge XAFS spectra were measured by RapidXAFS 1M (Anhui Absorption Spectroscopy Analysis Instrument Co. Ltd). All XAFS spectra were processed using the Ifeffit package. The nuclear magnetic resonance (^{1}H-NMR) spectrum was achieved on a Bruker spectrometer (400 MHz) in D_2O. In situ electrochemical FTIR spectroscopic was performed using a Fourier transform infrared spectrometer (Nicolet iS50), coupling with an in-situ electrochemical reaction cell (SPEC-I, Yuanfang Co. Ltd., Shanghai, China). The catalyst ink was dripped onto a hemicylindrical silicon prism covered with a layer of gold membrane. A platinum wire and Ag/AgCl electrode were used as counter and reference electrodes. During the test, CO_2 gas was constantly purged with CO_2. The background spectrum (reflectance R_0) was recorded at open circuit voltage. All spectra were reported as the relative change in reflectivity, $\Delta R/R_0 = (R-R_0)/R_0$. The R and R_0 are single-beam spectra collected at the applied bias and the reference potential.

Finite-element method simulations

Finite-element method (FEM) simulations were performed using the COMSOL Multiphysics software package. The 'Transport of Diluted Species' module was employed to comprehensively model the mass transport of two species within nanotubes. Molecular transport

was followed by Fick's law of diffusion, which expresses the diffusion flux, J_i in mol.m^{-2}.s^{-1} as proportional to the anti-gradient of the local concentration, c_i (in mol. m^{-3}) at a position vector r at time t[3]:

$$J_i = -D_i \nabla c_i(r,t)$$

where D_i symbolizes diffusion coefficient (in m^2 s^{-1}) and ∇ is the del operator.

The nanotube geometry used in the simulation was 2D axisymmetric, including an inflow port and an outflow port. Two different nanotube configurations were calculated, one with a length of 2 nm and another with a length of 300 nm, while both nanotubes have the same radius of 0.25 nm. The diffusion constants used in the simulations were 0.9423e-9 m^2/s for H_2O and 1.91e-9 m^2/s for CO_2 within nanotubes at a temperature of 298 K, which were obtained from the literature [4]. The initial concentrations of 55600 mol/m³ for H_2O and 33 mol/m³ for CO_2 were used at the inflow port of the nanotube. Finally, the concentration variation with time was analyzed at the outflow port of the nanotube.

DFT calculations

The Vienna ab initio Simulation Package (VASP) was employed to compute the Gibbs free energy and the density of states (DOS) of the systems under the framework of density functional theory[5]. The evaluation of the exchange-correlation energy was carried out using the generalized gradient approximation (GGA) with the Perdew-Burke-Ernzerhof (PBE) function[6]. To ensure accurate self-consistent charge density, a plane-wave basis set with an energy cutoff of 400 eV was utilized. Optimized geometries were identified by applying an atomic force convergence criterion of 0.001 eV Å^{-1}. The surface slab model was constructed with a generous vacuum space of 25 Å to prevent interactions between different slabs. Geometry optimizations were performed by sampling the Brillouin zone with a single gamma grid. The DFT-D3 dispersion correction method was used to account for the weak interaction between slabs and active species. The computational hydrogen electrode (CHE) model, as introduced by Nørskov and co-workers, was employed to calculate the Gibbs free energy of reactions involving electron/proton transfer[7]. The Gibbs free-energy change (ΔG) of elementary reaction is defined as follows:

$$\Delta G = E_{DFT} + E_{ZPE} - T\Delta S$$

To eliminate the effect of the solution environment, the solvation energy (E_{sol}) was corrected by GBRV ultrasoft pseudopotentials.

At the cathode surface, the reduction of CO_2 to produce CO could occur via the following elementary steps:

$$CO_2 + (H^+ + e^-) + * \rightarrow *COOH$$

$$*COOH + (H^+ + e^-) \rightarrow *CO + H_2O$$

$$*CO \rightarrow CO\uparrow + *$$

where * denotes the active sites on the catalyst surface[8]. Although H_2O was considered as the proton source, the H^+ was used directly for DFT calculation, because the H_2O dissociates into H^+ first before participating in CO_2RR.[9]

Results and Discussion

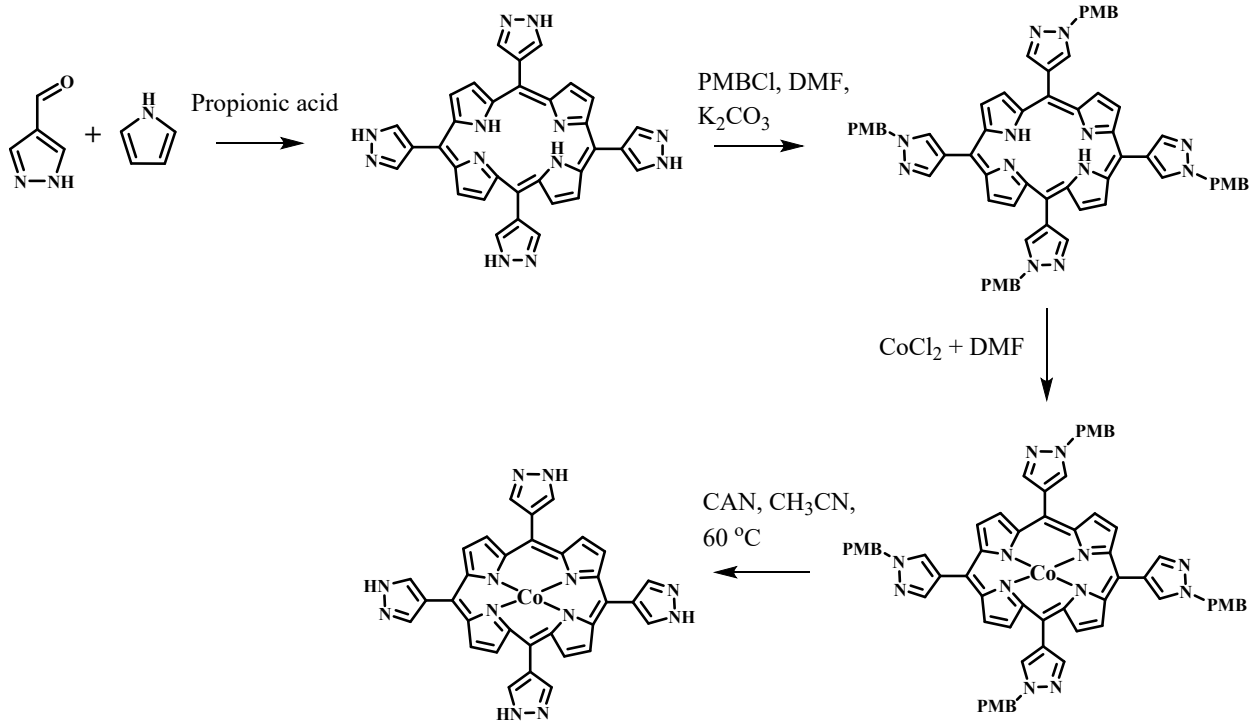

Figure S1. Synthesis route for the Co-TPP.

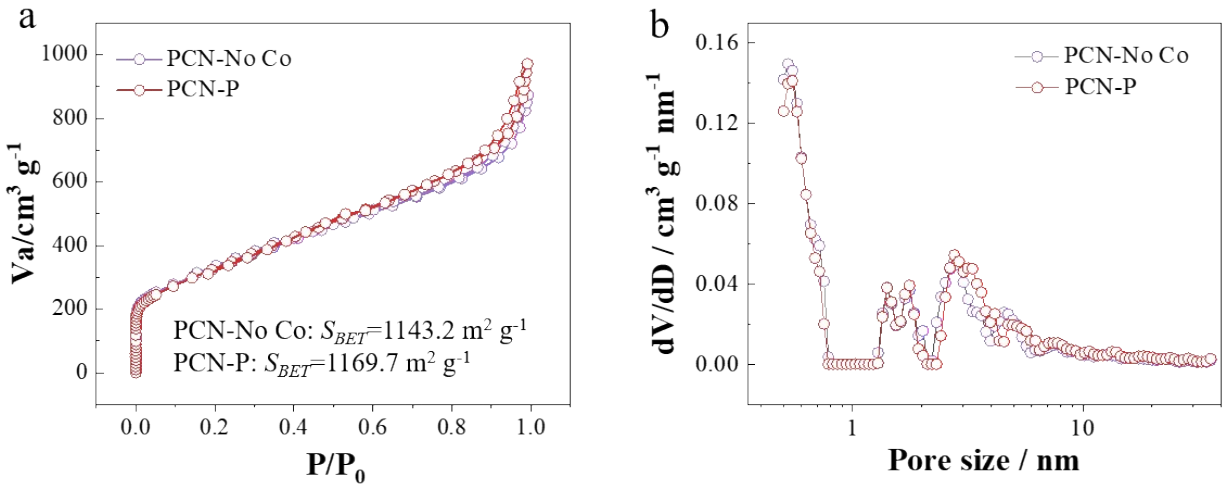

Figure S2. (a) N_2 adsorption-desorption plots of PCN-P and PCN-No Co, and (b) the corresponding pore size distribution curves.

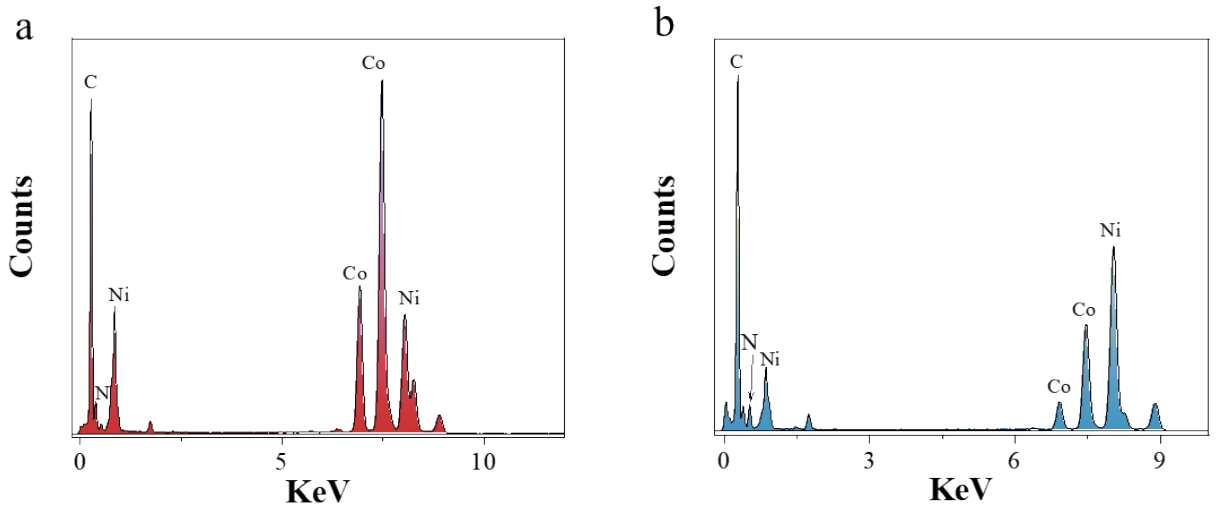

Figure S3. (a) EDS analysis for (a) PCN-P, and (b) PCN-QDs.

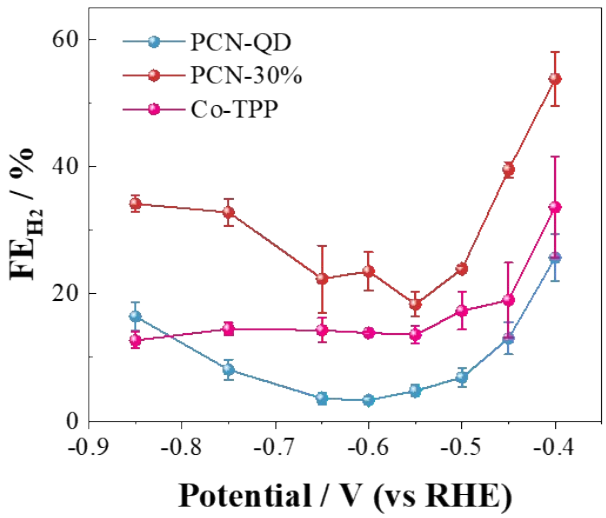

Figure S4. Faradaic efficiency of H_2 for PCN-QD, PCN-30%, and Co-TPP.

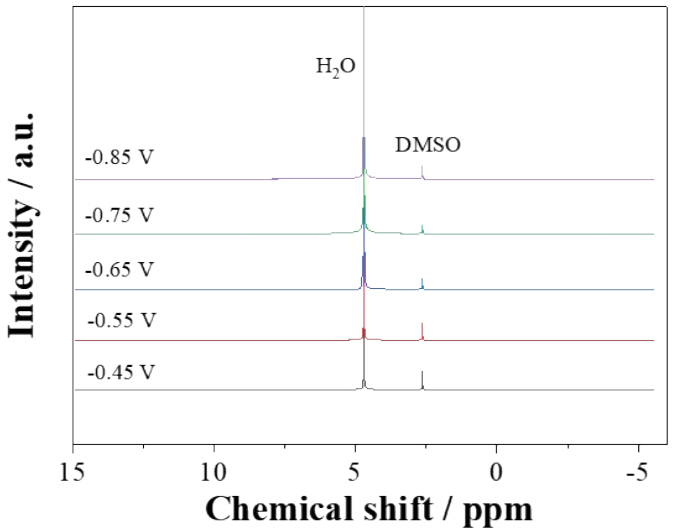

Figure S5. ^{1}H NMR spectra of the electrolyte after electrolysis at different potentials over PCN-QD.

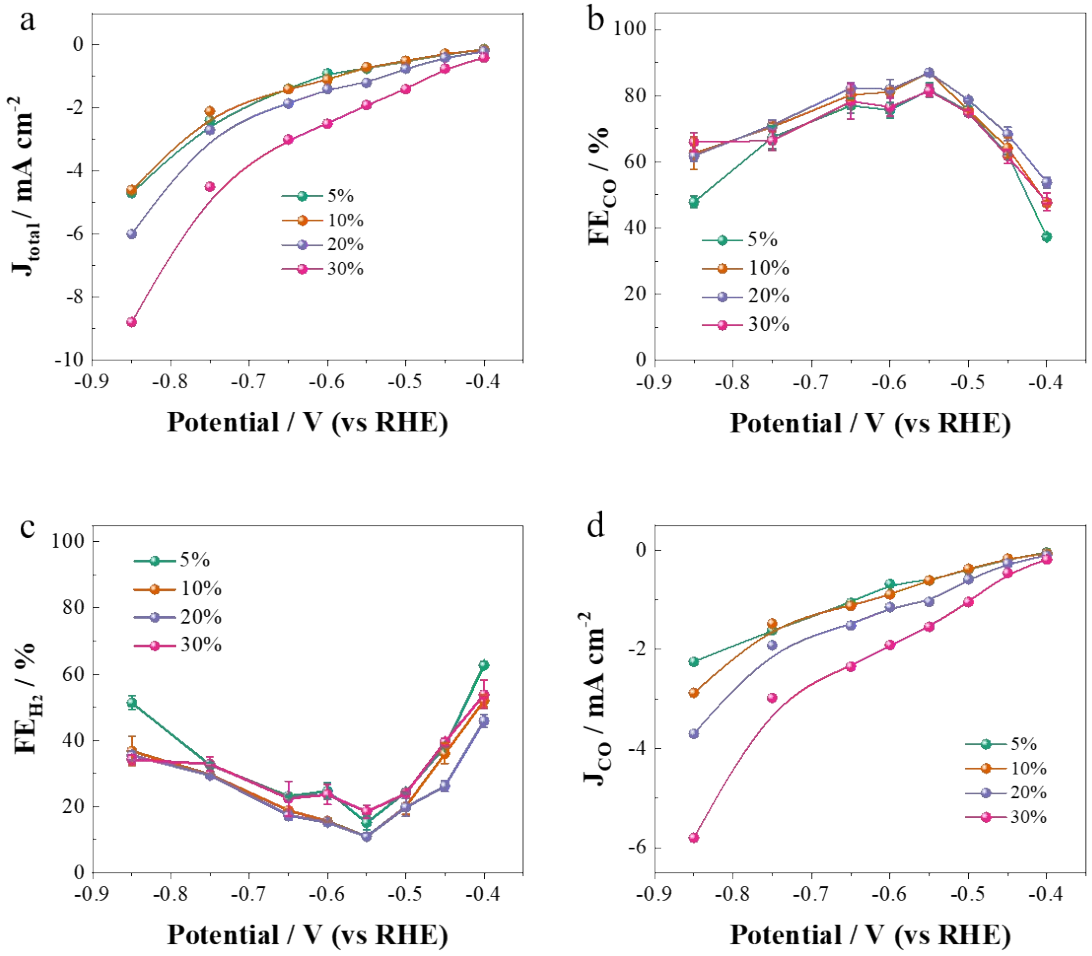

Figure S6. (a) Total current density, (b) FE_{CO}, (c) FE_{H2}, and (d) J_{CO} for electrocatalysts with different fractions of pristine PCN-P.

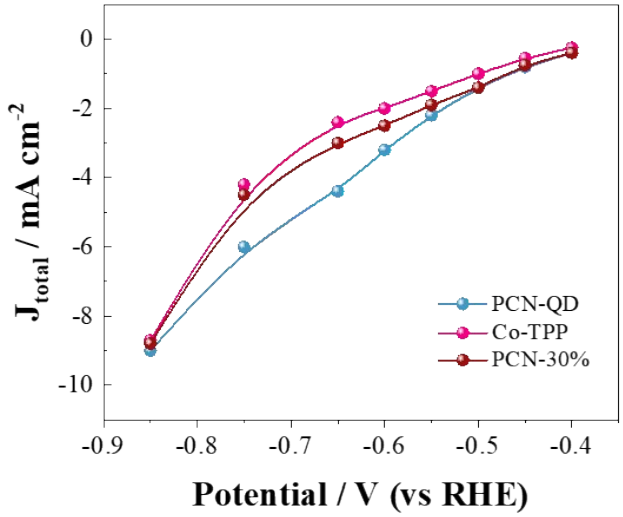

Figure S7. Total current density of PCN-QD, Co-TPP, and PCN-30%.

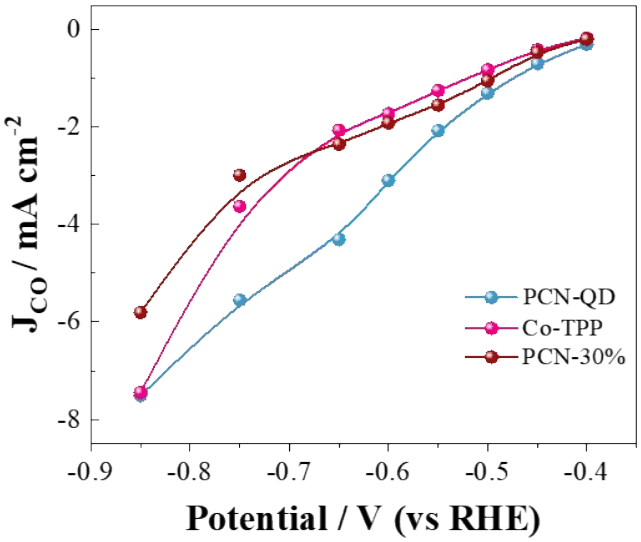

Figure S8. Partial current density of CO for PCN-QD, Co-TPP, and PCN-30%.

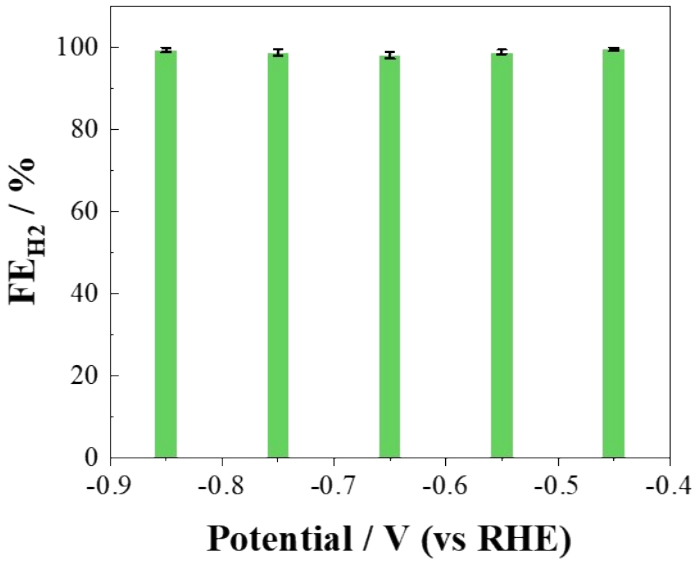

Figure S9. FE_{H2} of PCN-QD collected in N_2-saturated electrolyte.

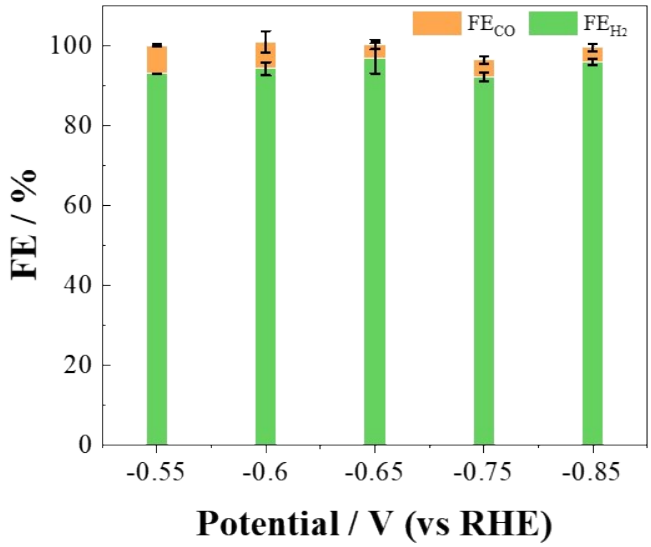

Figure S10. FE of CO and H_2 for activated carbon substrate.

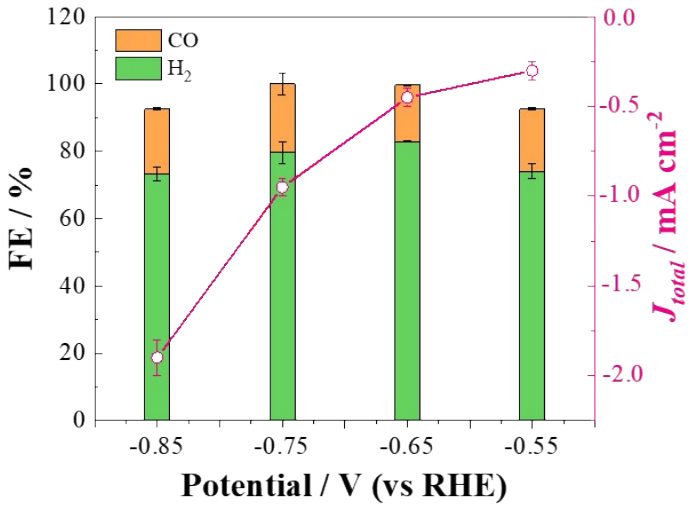

Figure S11. FE of CO and H_2 for PCN-601.

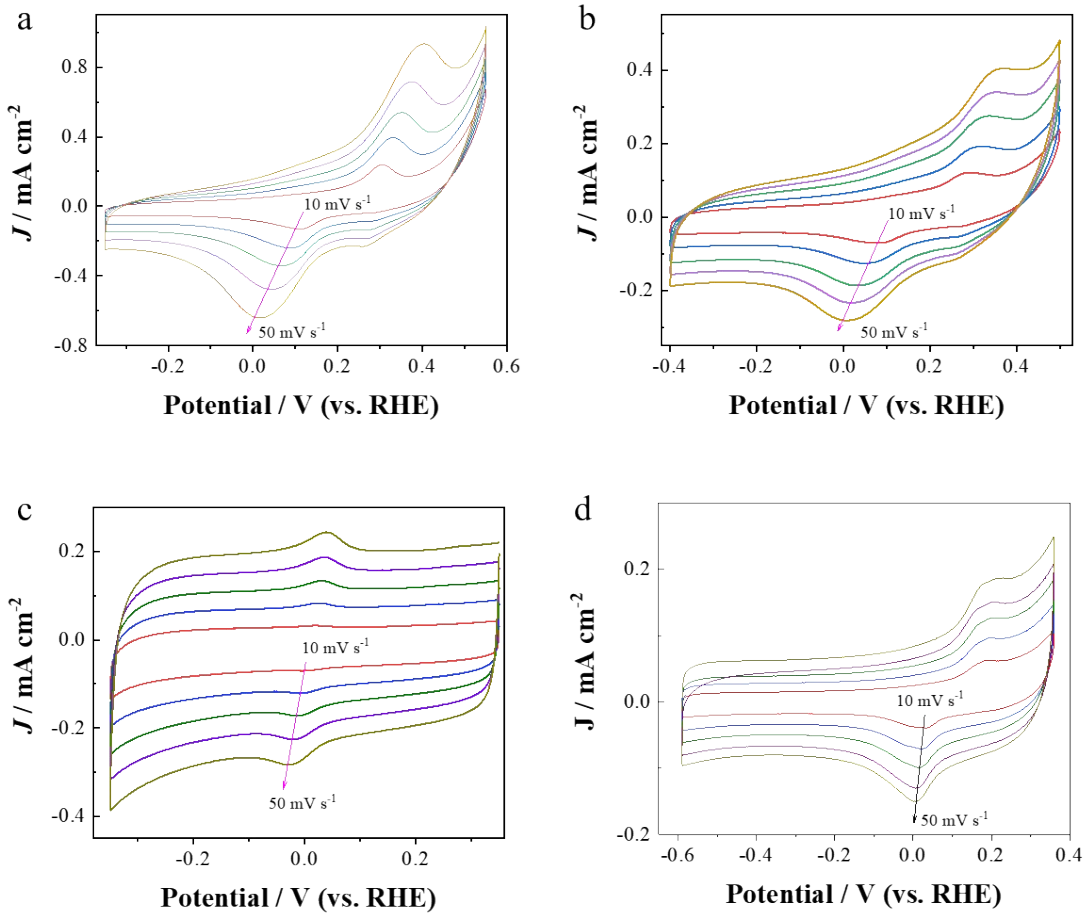

Figure S12. CV curves for the redox evaluation of Co site for (a) PCN-30%, (b) PCN-QD, (c) Co-TPP, and (d) PCN-5%.

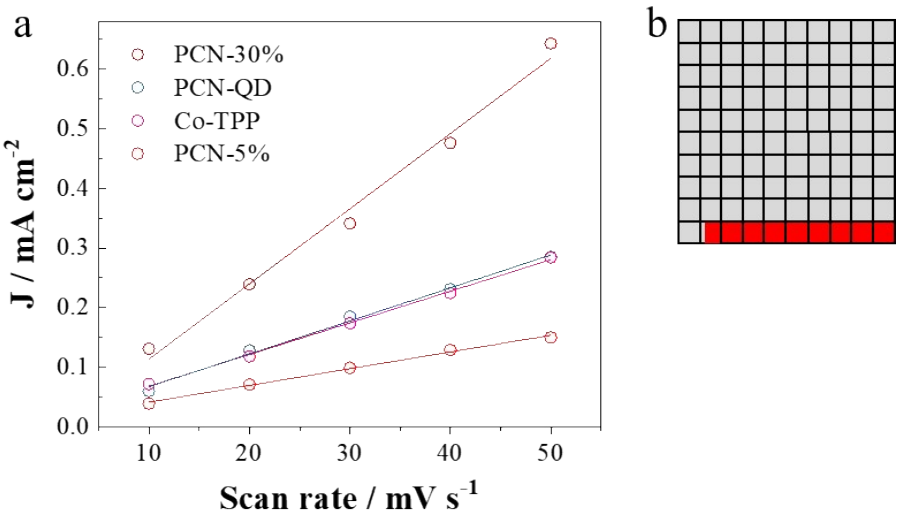

Figure S13. (a) The relationship between the scan rate and the current density for the reduction peak in the CV curves. (b) Utilization efficiency of single-atom Co site in PCN-5%.

Taking the PCN-QD as an example, we present the detailed calculation process for the utilization efficiency. As shown in **Figure S13**, the linear fitting result gave a slope of 0.00553 for the redox current at various scan rates.

$$\frac{i_{p,c}}{v} = slope = \frac{n^2F^2A\Gamma}{4RT}$$

$$0.00553\ \text{mA mV}^{-1}\ \text{s} = \frac{1^2 \times 96485^2 \times \text{A}^2\,\text{s}^2\,(\text{mol}^{-1})^2 \times 0.196\ \text{cm}^2 \times \Gamma}{4 \times 8.314\ \text{J mol}^{-1}\,\text{K}^{-1} \times 298\ \text{K}}$$

$$\Gamma = \frac{0.00553\ \text{A V}^{-1}\,\text{s} \times 4 \times 8.314\ \text{V A s} \times 298}{96485^2 \times \text{A}^2\,\text{s}^2\,\text{mol}^{-1} \times 0.196\ \text{cm}^2}$$

$$\Gamma = \frac{0.00553 \times 4 \times 8.314 \times 298}{96485^2 \times \text{mol}^{-1} \times 0.196\ \text{cm}^2} = 3.0 \times 10^{-8}\ \text{mol cm}^{-2}$$

Since the total content of Co atoms in PCN-QD is 0.38wt% as determined by ICP, the $Co_{utilized}$ can be calculated as follows, considering the loading of catalyst is 0.5 mg cm^{-2} in this work.

$$Co_{utilized} = \frac{\Gamma \times S \times M_{Co}}{m_{Co}}$$

$$= \frac{3.0 \times 10^{-8}\,mol\,cm^{-2} \times 1\,cm^2 \times 59\,g\,mol^{-1}}{0.5\,mg\,cm^{-2} \times 1\,cm^2 \times 0.38\%}$$

= 93.1%

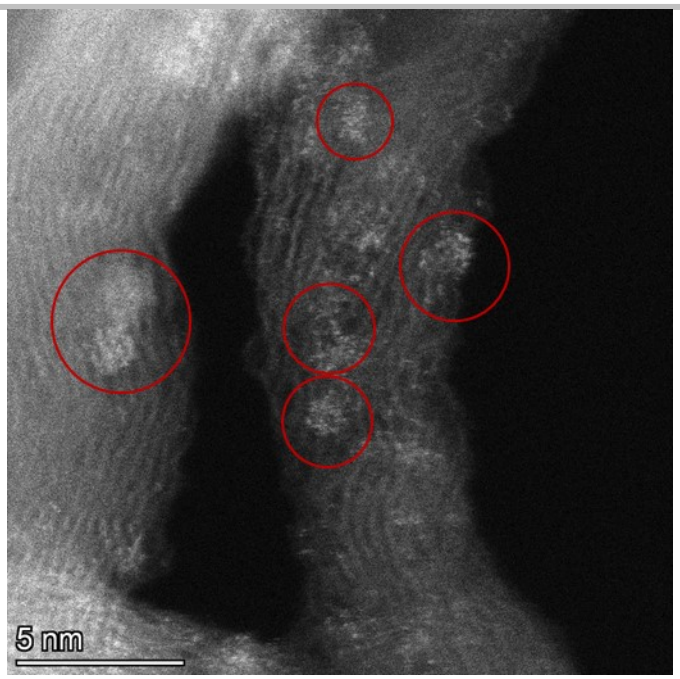

Figure S14. Spherical aberration-corrected transmission electron microscope image for Co-TPP.

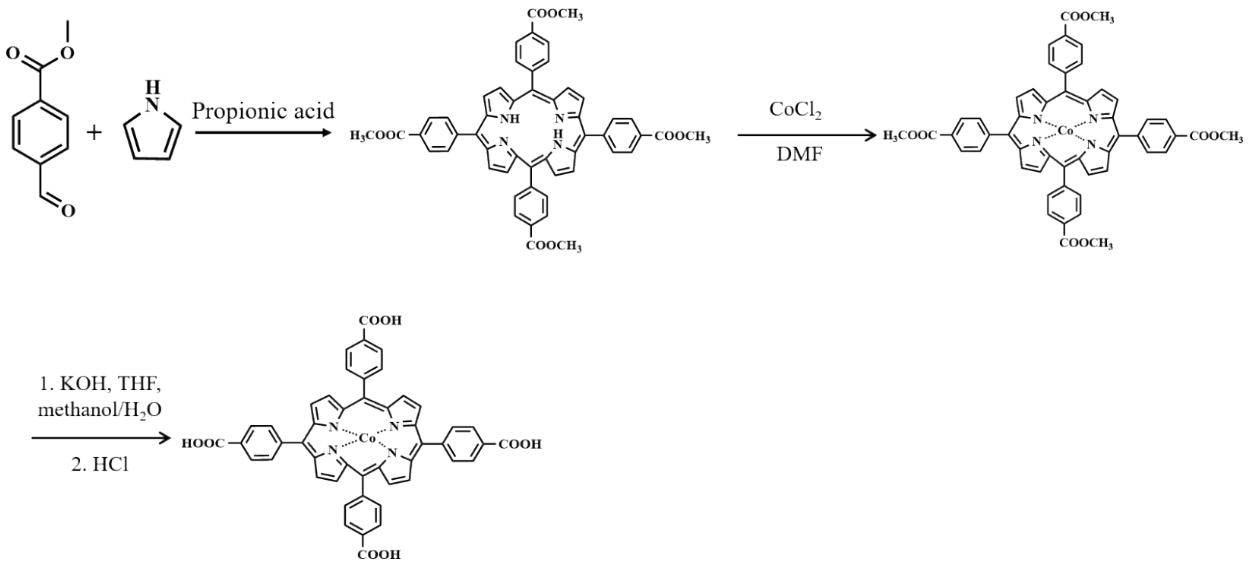

Figure S15. Synthesis route for the Co-TCPP.

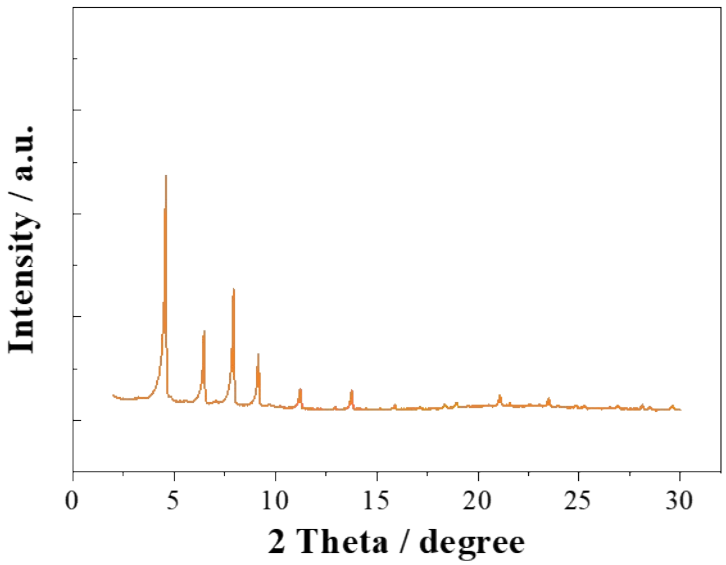

Figure S16. XRD pattern of PCN-224(Co).

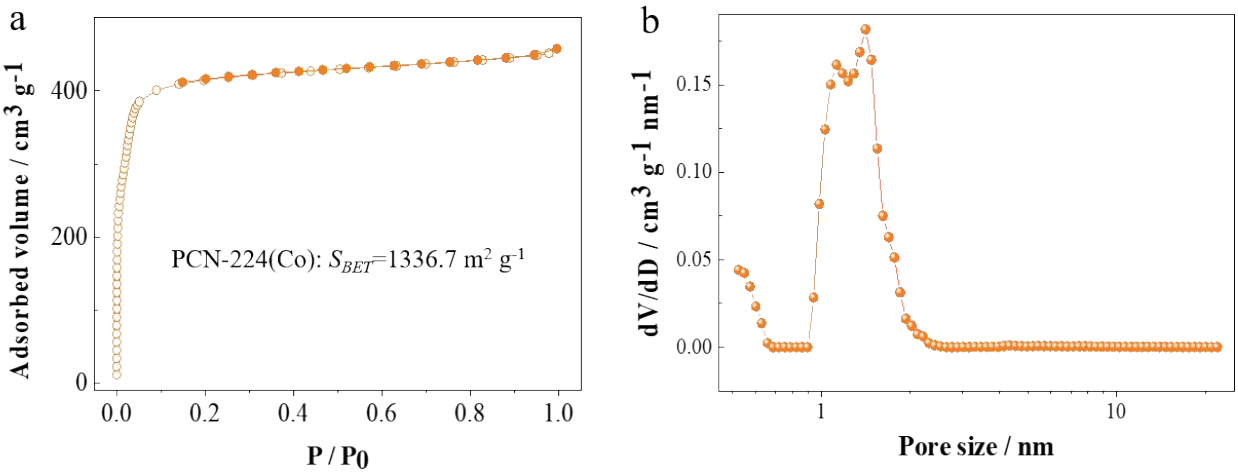

Figure S17. (a) N_2 adsorption-desorption curve, and (b) corresponding pore size distribution plot for PCN-224(Co).

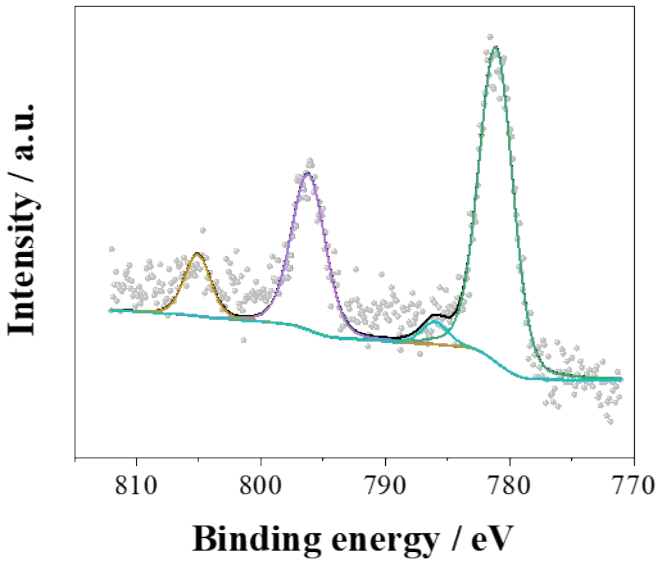

Figure S18. High-resolution XPS Co 2p spectrum for PCN-224(Co).

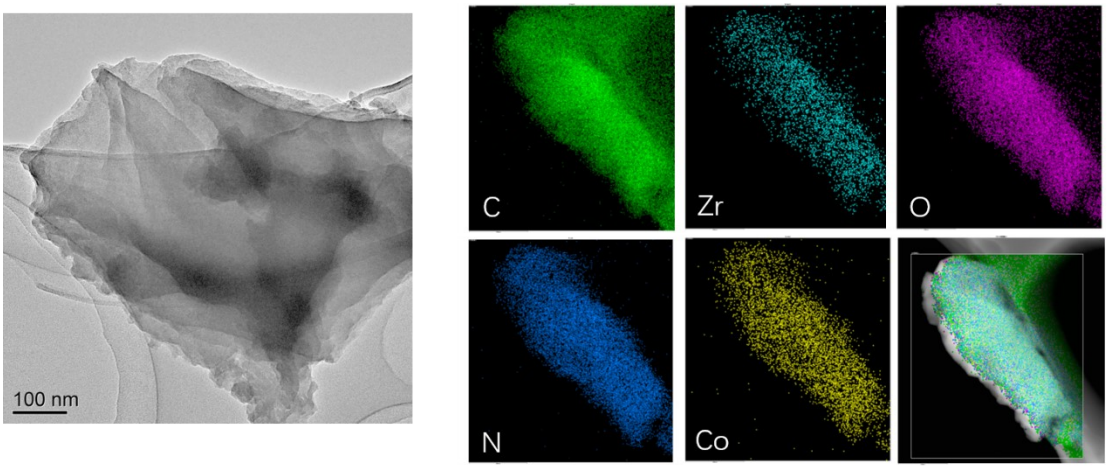

Figure S19. TEM image and element distribution of C, Zr, O, N, and Co for PCN-224(Co).

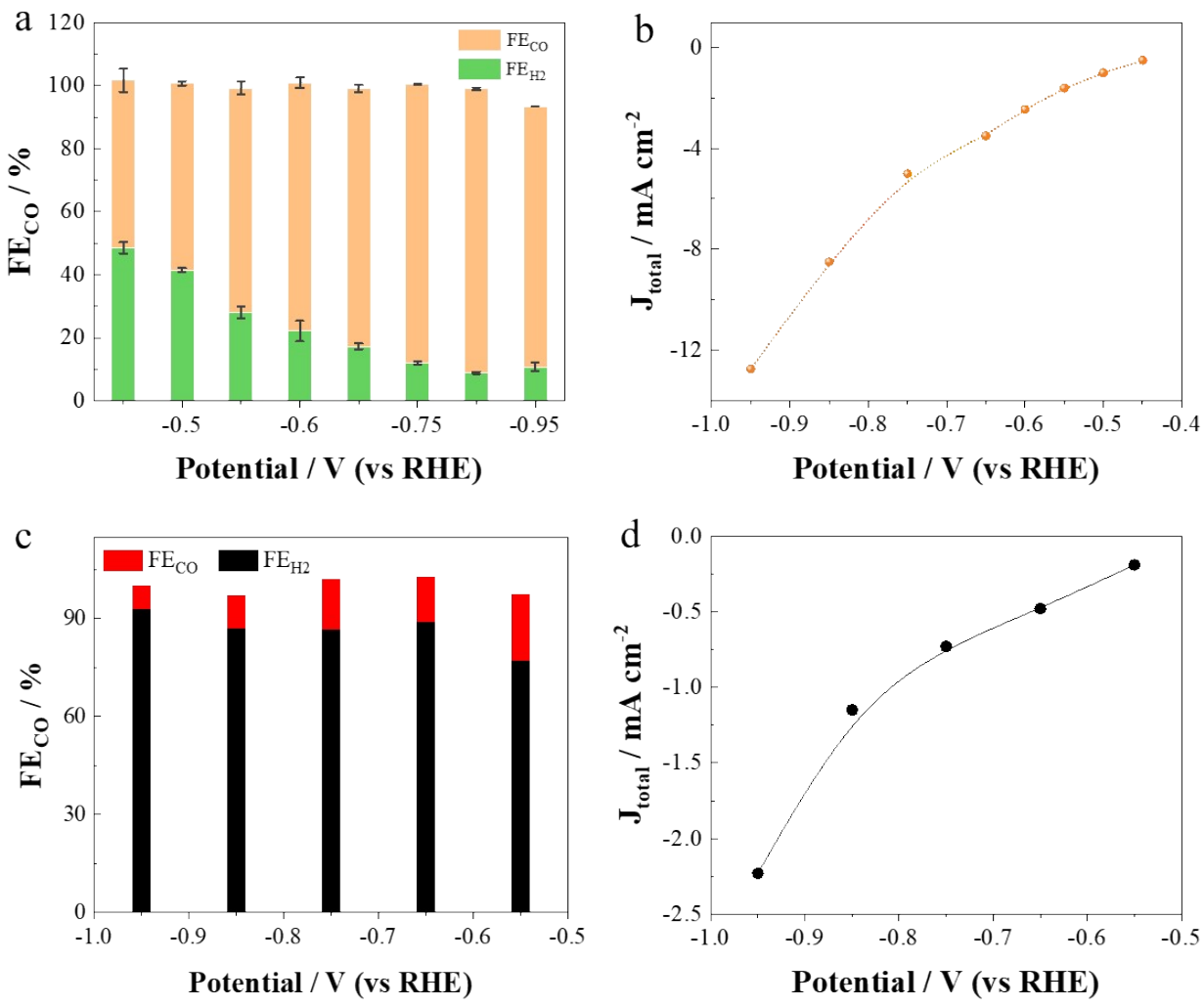

Figure S20. (a) FE of CO and H_2, and (b) corresponding total current density of PCN-224(Co). (c) FE of CO and H_2, and (d) total current density of PCN-224.

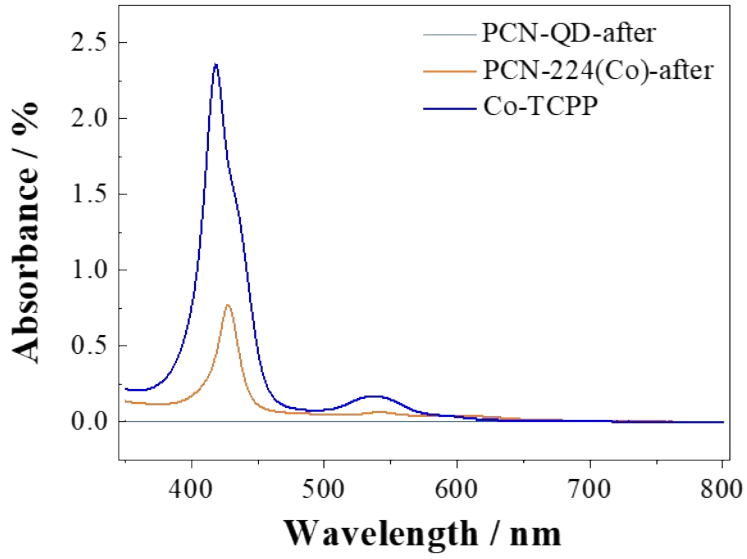

Figure S21. UV-vis for the electrolyte after electrolysis for PCN-QD and PCN-224(Co)-QD, as well as the Co-TCPP aqueous solution.

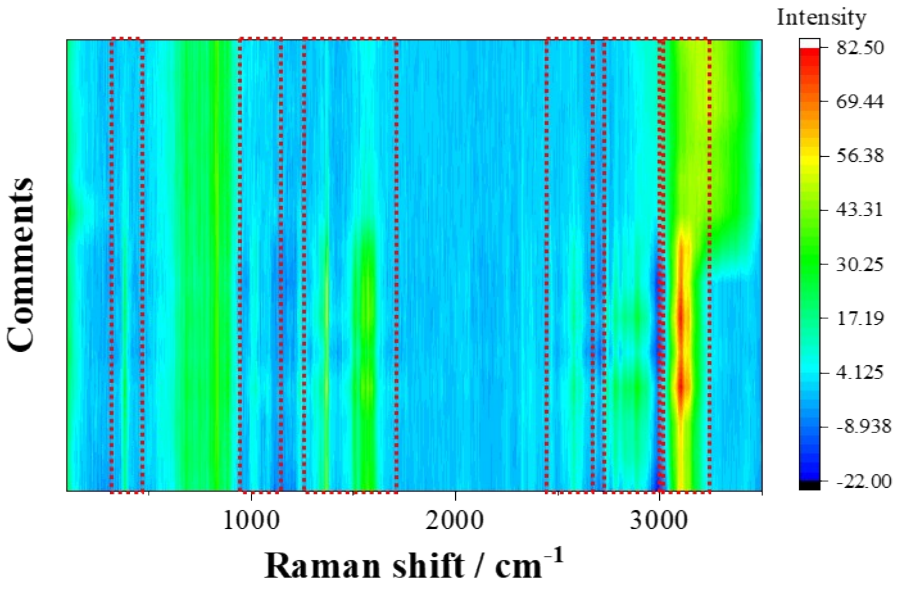

Figure S22. In situ Raman spectrum for PCN-224(Co)-QD.

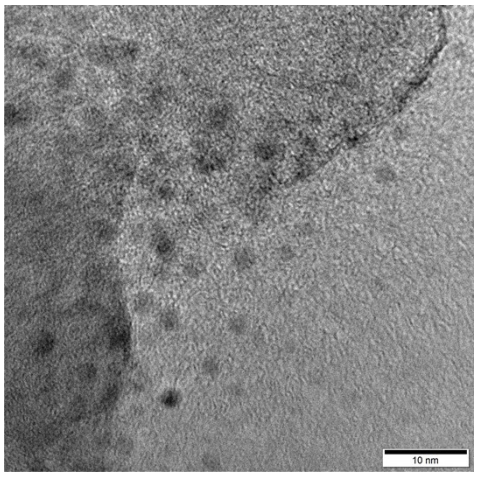

Figure S23. TEM image of PCN-QD catalyst after stability testing.

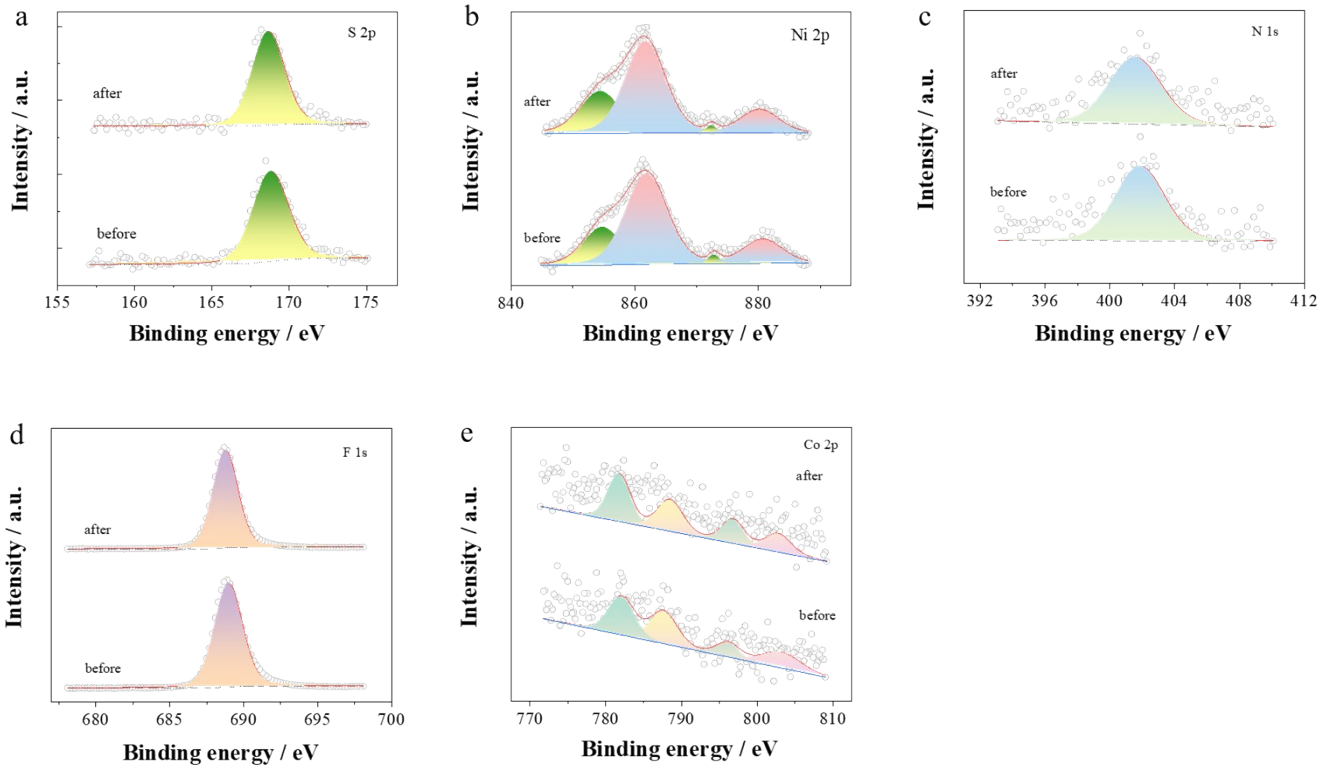

Figure S24. High-resolution XPS spectra of (a) S 2p, (b) Ni 2p, (c) N 1s, (d) F 1s, and (e) Co 2p.

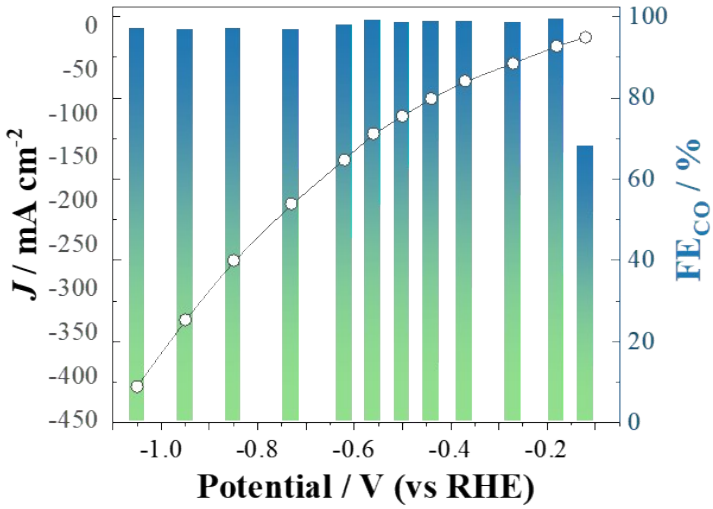

Figure S25. The current density and FE_{CO} of PCN-QD obtained by flow-cell.

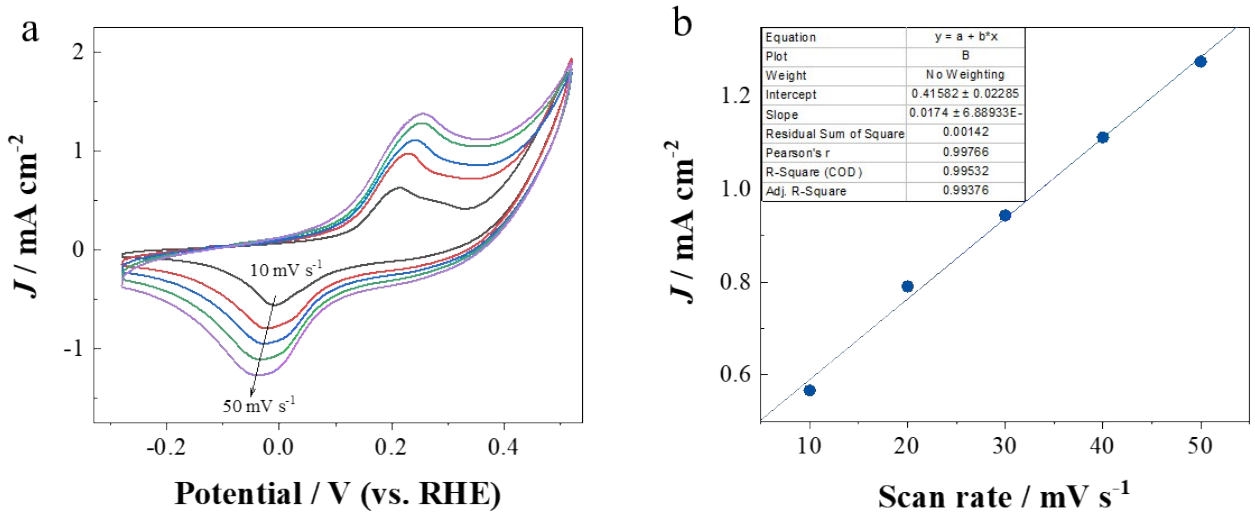

Figure S26. (a) The CV curves of PCN-QD-15% at different scan rates. (b) The corresponding redox current density at different scan rates. The inset is the linear fitting result for these data points.

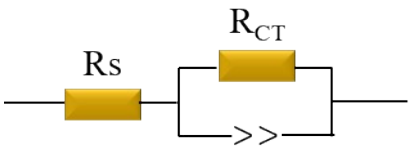

Figure S27. The equivalent circuit for EIS fitting.

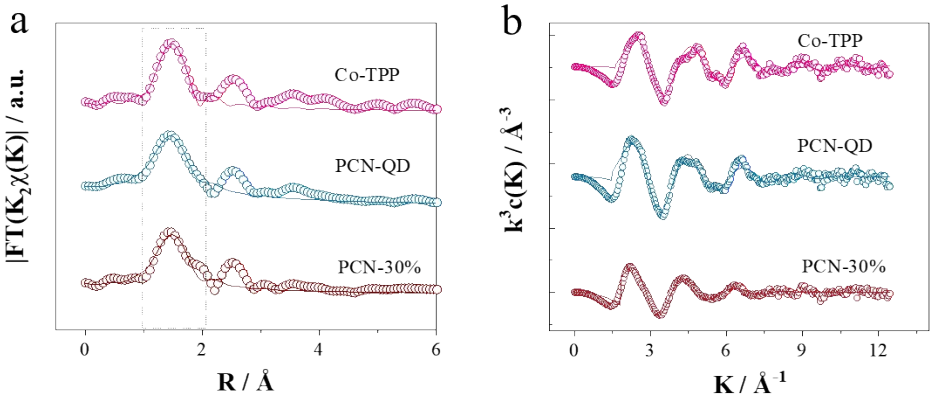

Figure S28. EXAFS fitting curve of PCN-30%, PCN-QD, and Co-TPP in (a) R, and (b) k space.

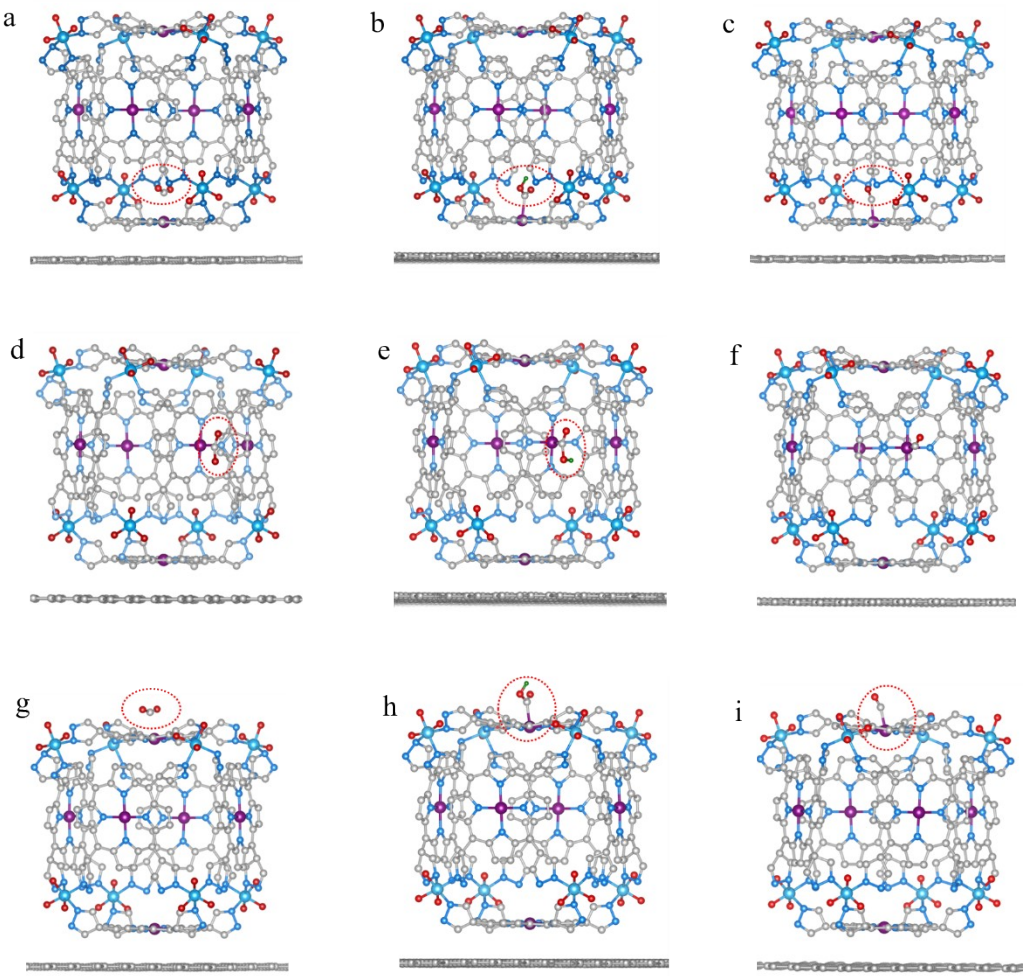

Figure S29. The adsorption configurations for (a) CO_2, (b) *COOH, and (c) *CO over down-Co site. (d) CO_2, (e) *COOH, and (f) *CO over side-Co site. (g) CO_2, (h) *COOH, and (i) *CO over top-Co site.

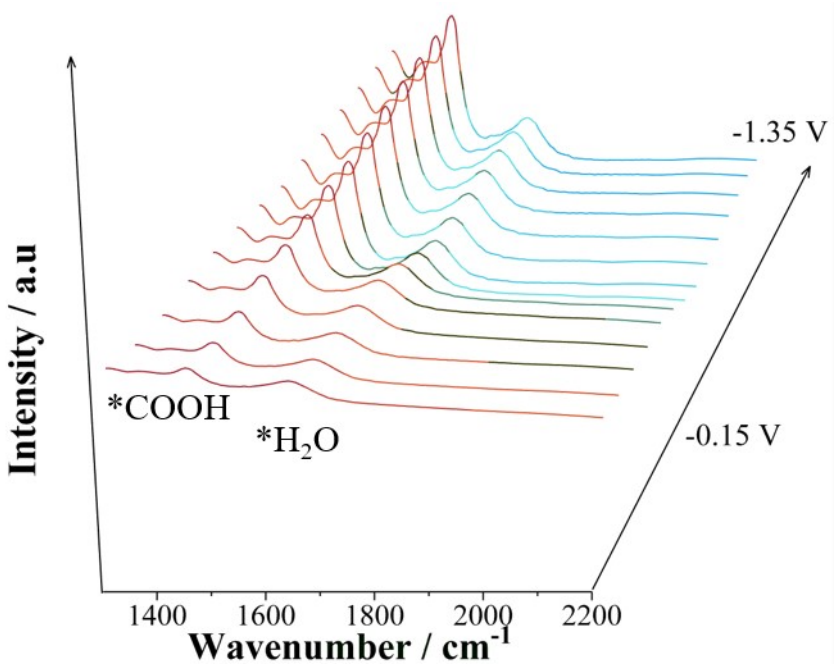

Figure S30. In situ ATR-SEIRAS of PCN-30%.

Table S1. Summary of the Co content, electrolyte, FE_{co}, J for Co-based single-atom catalysts. The label of flow indicates data collected by the flow cell.

Sample	Cowt%	electrolyte	FE_{co}/%	J/mA cm^{-2}	Reference
Co_1-$N_{4-x}C_x$	0.63	0.1 M $KHCO_3$	82	-15.8	*Appl. Catal. B*, 2019, **240**, 234.
CoPc@DNHCS-T		0.5 M $NaHCO_3$	95.68	-16.49	*Adv. Funct. Mater.*, 2022, **32**, 2110649.
N–C–CoPc NR	0.93(at)	0.1 M $KHCO_3$	85.3	-6	*ACS Appl. Energy Mater.* 2020, **3**, 3893.
Co-N-C	0.27	0.5 M $KHCO_3$ 1 M KOH	99.4 99.8(flow)	-24.8 -350(flow)	*ACS Catal.* 2022, **12**, 2513.
Co-N_2	0.25	0.5 M $KHCO_3$	94	-18.1	*Angew. Chem. Int. Ed.,* 2018, **57**, 1944.
CoN_4-CB		0.5 M $KHCO_3$ 1 M KOH	98.7 99(flow)	-33.6 -650(flow)	*Appl. Catal. B.,* 2022, **304**, 120958.
Co-N_5	3.54	0.2 M $NaHCO_3$	99.4	-4.5	*J. Am. Chem. Soc.,* 2018, **140**, 4218.
CoPc/C		0.5 M $KHCO_3$	85	-20.4	*ACS Catal.,* 2022, **12**, 14571.
CoPc		0.5 M $KHCO_3$	99	-20	*Angew. Chem. Int. Ed.,* 2018, **57**, 16339.
CoPcs		0.5 M $KHCO_3$	95	-10	*J. Am. Chem. Soc.* 2022, **144**, 16131.
CoPPCl/CNT	1	0.5 M $NaHCO_3$	90	-5.5	*Angew. Chem. Int. Ed.,* 2019, **58**, 6595.
U120-CoPc/KB	0.11	0.5 M $KHCO_3$	96.4	-44	*J. Phys. Chem. Lett.* 2023, **14**, 3844.
CoPc/CNT		1 M $NaHCO_3$	96	-2.5	*ACS Energy Lett.* 2018, **3**, 1381.
CoP@NrGO	2	0.5 M $NaHCO_3$	~90	~ -3.5	*ACS Appl. Energy Mater.* 2019, **2**, 2435.
CoPc@HCS	1.26	0.5 M $KHCO_3$	91	-14	*Nano Energy*, 2021, **84**, 105904.
PCo/Graphene		0.1 M $KHCO_3$	~92	-5	*Angew. Chem. Int. Ed.,* 2020, **59**, 19162.
CoPc/Graphene		0.1 M $KHCO_3$	80	-17	*ACS Energy Lett.* 2019, **4**, 666.
TcPcCo	1.27	0.5 M $KHCO_3$	99.3	~ -17	*Electro. Acta,* 2023, **441**, 141800.
Co(III)-N_4	5	0.5 M $KHCO_3$	97 99(flow)	-8.2 -191(flow)	*J. Am. Chem. Soc.* 2022, **144**, 1502.
CoTAP-cov		0.5 M $KHCO_3$	~100	~6	*Appl. Catal. B.*, 2022, **300**, 120750.
CoDAP/CNT		0.1 M $KHCO_3$	99	-20	*Green Chem.,* 2023, **25**, 10366.
CoTPyPP		0.5 M $KHCO_3$	95	-20	*ChemSusChem,* 2021, **14**, 2126.
CoPc-ZIS		0.5 M $KHCO_3$	93	-8	*Chem. Sci.,* 2019, **10**, 1659.
CoTPP		0.5 M $KHCO_3$	90	-3.2	*Angew. Chem. Int. Ed.,* 2017, **56**, 6468.
CoPc		0.1 M $KHCO_3$	99	-3	*Nano Energy,* 2020, **67**, 104163.
Co^{II}CPY/CNT		0.1 M $KHCO_3$	98	-23	*Adv. Energy. Mater.,* 2022, **12**, 2022108.
CoPc-COOH/NH_2-CNT		0.5 M $KHCO_3$	91	-22.4	*Nano Res.,* 2023, **16**, 3649.
CoPc/CNT	2.5	0.1 M $KHCO_3$	95	-10	*Nat. Commun.,* 2017, **8**, 14675.
CoPc/MQD-OH	4.34	0.1 M $KHCO_3$	~100	-18	*ACS Appl. Mater. Interface,* 2023, **15**, 24346.
CoPc		0.5 M $NaHCO_3$	95	-165(flow)	*Nat. Commun.,* 2019, **10**, 3602.
CoPc/CNT-MD	2.62	0.5 M $KHCO_3$	97	-200(flow)	*Adv. Funct. Mater.,* 2022, **32**, 2107301.
CoPPc-CNT	5.6	0.5M $NaHCO_3$	90	-4	*Green Chem.,* 2019, **21**, 6056.
CoPc-P4VP		0.1 M	90	-2.5	*Chem. Sci.,* 2016, **7**,

		NaH_2PO_4			2506.
Co-PorN_3/CNT	4.12	0.5 M $KHCO_3$	96	~-30	*Small*, 2021, **17**, 2102957.
Hg-CoTPP		1 M $KHCO_3$ 1 M KOH	95.6 98.9	-31 -1200	*J. Am. Chem. Soc.* 2022, **144**, 15143.
Co SAs/Zr-CPF		0.1 M $KHCO_3$	76.8	-5	*Nano Lett.* 2022, **22**, 3340.
Co-PPOLs	10.3	0.1 M $KHCO_3$	94.2	-6 -200(flow)	*Angew. Chem. Int. Ed.,* 2023, **62**, e202219241.
MOL-Co-Nx		1 M $KHCO_3$	99	-2.5	*J. Am. Chem. Soc.,* 2020, **142**, 21493.
COF-367-Co	10	0.5 M $KHCO_3$	90	-9	*Science,* 2015, **349**, 1208.
Co-iBFBim-COF-X	4.91	MEA	99	-45(flow)	*Angew. Chem. Int. Ed.,* 2023, **135**, e202215687.
CoTAP-iCONs	4.1	1 M KOH	95	-212(flow)	*Angew. Chem. Int. Ed.,* 2022, **34**, 2110496.
TCPP(Co)/Zr-BTB		0.5 M $KHCO_3$	85.1	-6	*Chem-Eur J.,* 2020, **26**, 1604.
1-NH_2-Co	1	0.1 M NaH_2PO_4	99.4	-7.2	*CCS Chem.,* 2022, **5**, 145.
3D-Por(Co/H)-COF	0.56	0.5 M $KHCO_3$	92.4	-15.5	*J. Mater. Chem. A,* 2022, **10**, 4653.
TTF-Por(Co)-COF	3.73	0.5 M $KHCO_3$	95	-6.88	*ACS Energy Lett.* 2020, **5**, 1005.
TAPP(Co)-B18C6-COF	3.0	0.5 M $KHCO_3$	93.2	-9.45	*ACS Energy Lett.* 2021, **6**, 3496.
CoPc-PI-COF	3.7	0.5 M $KHCO_3$	97	-21.2	*J. Am. Chem. Soc.* 2021, **143**, 7104.
CoPc-PI-COF-3	5.1	0.5 M $KHCO_3$	96	-31.7	*Angew. Chem. Int. Ed.,* 2022, 6**1**, e202114244.
Por(Co)-COF	4.16	0.5 M $KHCO_3$	91.4	-7.8	*Small,* 2021, **17**, 2004933.
CoPc-H_2Por	3.78	0.5 M $KHCO_3$	90	-19	*Adv. Mater.* 2022, **34**, 2203139.
CoCp2@MOF-545-Co	2.52	0.5 M $KHCO_3$	97	-25	*Nano Energy,* 2020, **67**, 104233.
Co-CTF	0.13(at)	0.1 M $KHCO_3$	85	< -2	*Chem. Sci.,* 2018, **9**, 3941.
CoPc-PDQ-COF	4.35	0.5 M $KHCO_3$	96	-49.4	*Angew. Chem. Int. Ed.,* 2020, **59**, 16587.
366-F-Co		0.5 M $KHCO_3$	87	-65 mA mg^{-1}	*J. Am. Chem. Soc.* 2018, **140**, 1116.
TPY-MOL-CoPP		0.1 M $NaHCO_3$	92.2	-1314 mA mg^{-1}	*J. Am. Chem. Soc.* 2019, **141**, 17875.
Co-PMOF		0.5 M $KHCO_3$	99	-11.6	*Nat. Commun.,* 2018, **9**, 4466.
Co-TTCOFs	3.4	0.5 M $KHCO_3$	99.7	-4	*Nat. Commun.,* 2020, **11**, 497.
MOF-NS-Co	3.64	0.1 M $KHCO_3$	98.7	-7.2	*Small Methods,* 2020, **5**, 2000991.
PCN-QD PCN-QD-15%	0.38	0.1 M $KHCO_3$ 1 M KOH 1 M KOH	97.9 99.6 99.57	-9.0 -408.8 (flow cell) -950 (flow cell)	This work

Table S2. Fitting parameters of Co K-edge EXAFS spectra.

Sample	Path	N	R / Å	σ^2 / Å^2	R factor
Co-TPP	Co-N	3.8	1.88	0.007	0.025
PCN-30%	Co-N	4.3	1.87	0.009	0.039
PCN-QD	Co-N	4.2	1.88	0.004	0.028

References

[1] K. C. Wang, X. L. Lv, D. W. Feng, J. Li, S. M. Chen, J. L. Sun, L. Song, Y. B. Xie, J. R. Li, H. C. Zhou, *J. Am. Chem. Soc.* **2016**, *138*, 914-919.

[2] aP. L. Taberna, P. Simon, J. F. Fauvarque, *J. Electrochem. Soc.* **2003**, *150*, A292-A300; bS. H. Lee, J. Kim, D. Y. Chung, J. M. Yoo, H. S. Lee, M. J. Kim, B. S. Mun, S. G. Kwon, Y. E. Sung, T. Hyeon, *J. Am. Chem. Soc.* **2019**, *141*, 2035-2045.

[3] R. Gaur, L. Mishra, S. K. Sen Gupta, *Modelling and simulation of diffusive processes: methods and applications* **2014**, 27-49.

[4] aY. Liu, Q. Wang, *Physical review B* **2005**, *72*, 085420; bA. Striolo, *Nano letters* **2006**, *6*, 633-639.

[5] G. Kresse, D. Joubert, *Phys. Rev. B* **1999**, *59*, 1758-1775.

[6] J. P. Perdew, K. Burke, M. Emzerhof, *Phys. Rev. Lett.* **1996**, *77*, 3865-3868.

[7] aJ. Rossmeisl, Z. W. Qu, H. Zhu, G. J. Kroes, J. K. Norskov, *J. Electroanal. Chem.* **2007**, *607*, 83-89; bJ. Rossmeisl, A. Logadottir, J. K. Norskov, *Chem. Phys.* **2005**, *319*, 178-184; cI. C. Man, H. Y. Su, F. Calle-Vallejo, H. A. Hansen, J. I. Martinez, N. G. Inoglu, J. Kitchin, T. F. Jaramillo, J. K. Norskov, J. Rossmeisl, *Chemcatchem* **2011**, *3*, 1159-1165.

[8] aJ. B. Zhu, M. L. Xiao, D. Z. Ren, R. Gao, X. Z. Liu, Z. Zhang, D. Luo, W. Xing, D. Su, A. P. Yu, Z. W. Chen, *J. Am. Chem. Soc.* **2022**, *144*, 9661-9671; bH. A. Hansen, C. Shi, A. C. Lausche, A. A. Peterson, J. K. Norskov, *Phys. Chem. Chem. Phys.* **2016**, *18*, 9194-9201; cS. Sarfraz, A. T. Garcia-Esparza, A. Jedidi, L. Cavallo, K. Takanabe, *ACS Catal.* **2016**, *6*, 2842-2851; dW. H. Ren, X. Tan, C. Jia, A. Krammer, Q. Sun, J. T. Qu, S. C. Smith, A. Schueler, X. L. Hu, C. Zhao, *Angew. Chem. Int. Ed.* **2022**, *61*, e202203335.

[9] aJ. Y. Chen, Z. J. Li, X. Y. Wang, X. H. Sang, S. X. Zheng, S. J. Liu, B. Yang, Q. H. Zhang, L. C. Lei, L. M. Dai, Y. Hou, *Angew. Chem. Int. Ed.* **2022**, *61*, e202111683; bW. P. Ni, Y. J. Guan, H. J. Chen, Y. Zhang, S. Y. Wang, S. G. Zhang, *Angew. Chem. Int. Ed.* **2023**, *62*, e202303233; cM. C. Luo, Z. Y. Wang, Y. G. C. Li, J. Li, F. W. Li, Y. W. Lum, D. H. Nam, B. Chen, J. Wicks, A. N. Xu, T. T. Zhuang, W. R. Leow, X. Wang, C. T. Dinh, Y. Wang, Y. H. Wang, D. Sinton, E. H. Sargent, *Nat. Commun.* **2019**, *10*, 5814.